molbank

MDPI

Communication

Activation–Deactivation of Inter-Peptide Bond in Fluoro-*N*-(2-hydroxy-5-methyl phenyl)benzamide Isomers, Induced by the Position of the Halogen Atom in the Benzene Ring

Rodolfo Moreno-Fuquen [1,*], Nory Mariño-Ocampo [2], Juan Carlos Tenorio [3], Javier Ellena [4] and Alan R. Kennedy [5]

1 Department of Chemistry, Universidad del Valle, Santiago de Cali A.A. 25360, Colombia
2 Laboratorio de Química Supramolecular y Fotobiología, Departamento de Química Física, Escuela de Química, Facultad de Química y de Farmacia, Pontificia Universidad Católica de Chile, Vicuña Mackenna, Macul, Santiago 4860, Chile; njmarino@uc.cl
3 Instituto de Física, Universidade Federal do Rio de Janeiro, Rio de Janeiro CEP. 21941-909, Brazil; juandetenorio@yahoo.com
4 Instituto de Física de São Carlos, Universidade de São Paulo, São Carlos CEP. 13566-590, Brazil; javiere@ifsc.usp.br
5 WestCHEM, Department of Pure and Applied Chemistry, University of Strathclyde, 295 Cathedral Street, Glasgow G1 1XL, UK; a.r.kennedy@strath.ac.uk
* Correspondence: rodolfo.moreno@correounivalle.edu.co

check for updates

Citation: Moreno-Fuquen, R.; Mariño-Ocampo, N.; Tenorio, J.C.; Ellena, J.; Kennedy, A.R. Activation–Deactivation of Inter-Peptide Bond in Fluoro-*N*-(2-hydroxy-5-methyl phenyl)benzamide Isomers, Induced by the Position of the Halogen Atom in the Benzene Ring. *Molbank* **2022**, *2022*, M1416. https://doi.org/10.3390/M1416

Academic Editor: René T. Boeré

Received: 25 June 2022
Accepted: 27 July 2022
Published: 29 July 2022

Publisher's Note: MDPI stays neutral with regard to jurisdictional claims in published maps and institutional affiliations.

Abstract: The synthesis and XRD characterization at 295 K of three isomers, X-fluoro-N-(2-hydroxy-5-methyl phenyl) benzamide: (***o*-FPhB**), (***m*-FPhB**), and (***p*-FPhB**), are presented. ***o*-FPhB** and ***m*-FPhB** show high structural affinity concerning molecular and packing structures. The planarity of the C1-C7(O1)-N1-C8 peptide bond in ***o*-FPhB**, and ***m*-FPhB** confers high stability, favoring its tendency to acquire a resonant structure in the peptide segment and in the molecule. For ***p*-FPhB**, a stereochemical gate opens, leading to the activation of N-H···O interpeptide bonds, defining its supramolecular properties. Active participation of the halogen in the assembly of the structures is observed, forming intramolecular rings and molecule chains during crystal growth. The ***o*-FPhB** and ***m*-FPhB** form parallel sheets that develop hydrogen C-H···Cg, halogen C-F···Cg, or C=O···Cg interactions. Theoretical evaluations of the properties performed by the DFT/B3LYP/(6-311G(d,p) showed good agreement with the experimental values. The IR analysis reaffirms the presence of N-H, C=O, O-H, C-F, and C-H. In the UV-Vis, an increase in the energetic stability, O···H interactions, and electrostatic potential in the NH region reaffirm the disposition of ***p*-FPhB** for the formation of the N-H···O interpeptide bond. A molecular docking on the benzamides involving protein receptors showed similar behavior for all three isomers.

Keywords: crystal structure; fluorobenzamide; Hirshfeld surface; MEP; molecular docking

1. Introduction

The relevance of the amide group, with the presence of the fluorine atom, in antivirus activities was reported [1]. Fluorine is the most electronegative element in the periodic table, with a small atomic radius, resulting in exceptionally low polarizability. Although fluorine is rarely found in natural products, it is a common substituent and functional group in compounds related to the pharmaceutical and agrochemical industries [2]. The C–F bond is one of the strongest covalent bonds, with high average bond energies, and is often associated with relative metabolic inertia [3]. Fluorinated aromatic heterocycle compounds have gained significant attention in medicinal chemistry due to the solid electron-withdrawing nature of fluorine substituents and fluorine's ability to increase lipophilicity in drugs [4,5]

or to alter binding affinities with enzymes and receptors [6]. A previous structural study involving non-fluorinated N-(2-hydroxy)-5-methyl phenyl) benzamide (**PhB**) [7] prompted us to investigate congeners with fluorine as a substituent at different positions in the benzamide ring (A-ring). In this work, we propose the determination of the crystal structure of the isomers, ***o*-FPhB**, ***m*-FPhB**, and ***p*-FPhB**, to show how the position of the fluorine atom in the ring affects the properties of the interpeptide bonds influencing the organization of the crystal structure, through the formation of hydrogen bonds, halogen bonds, or short interactions where the halogen atom acts, thus visualizing the role that fluorine atoms can play in ligand–protein interactions. Results from parallel theoretical calculations will enable comparisons with the experimental results. This analysis will be helpful when designing new fluorinated systems that may have applications in areas such as medicine, pharmaceutics, or biochemistry.

2. Results

The synthesis of the fluorinated benzamides was adapted from a synthetic route that used acyl chlorides with different primary or secondary amines as nucleophiles [8]. The analysis by X-ray diffraction and spectroscopic studies enabled the three-dimensional structural elucidation of the three isomeric compounds. A supramolecular study of each compound was performed to analyze the different non-covalent intra–intermolecular interactions that each isomer presents. In addition, a survey of Hirshfeld surfaces [9] with their 2D representations, which are called fingerprints of these interactions, was undertaken. The analysis of these surfaces can reaffirm the behavior of intermolecular interactions in the crystalline system. The compounds under study were characterized by infrared spectroscopy to verify the presence of the amido and carbonyl functional groups indicating the formation of the N-phenyl-benzamides of interest and to find any spectroscopic information that could characterize in more detail the properties of the isomers treated in this work.

2.1. Structural Analysis

All three structures show similar melting points, same space group, and similar cell parameters for ortho and meta isomers (see Table S1). The Rint values showed excellent crystal quality in the diffraction process at 295 K. The ORTEP [10] diagrams of the isomers are shown in Figure 1, where an excellent response in their anisotropic thermal vibration parameters of the atoms is highlighted. The unit cell volumes for ***o*-FPhB** and ***m*-FPhB** are close, but a slight increase in volume is observed for ***p*-FPhB**. This tendency of ***p*-FPhB** to differentiate from the other two structures is also reflected in the change of the single crystallographic axis b, from the long axis to the shorter axis.

The most sensitive region to structural changes in these molecules could be the central C1-C7(O1)-N1-C8 peptide segment. The central moiety's bond distance and angle parameters do not undergo notable changes due to the different positions taken by the substituent F in the A-ring. The analysis of the intermolecular interactions through the formation of hydrogen and halogen bonds shows, in Table 1, a similar behavior for the O-H···O, C-H···O, and C-H···F bonds for ***o*-FPhB** and ***m*-FPhB** isomers; however, in the new arrangement of ***p*-FPhB**, the C2-H2···O2 bonds are strengthened, and the C6-H6···O2 bonds are weakened, resulting in the disappearance of the $R^2_2(7)$ rings, thus distorting the peptide bond and losing its resonant properties, its double bond character, making it more susceptible to nucleophilic or electrophilic attacks. This particular behavior is revealed in the appearance of interpeptide N-H···O bonds that integrate the crystalline arrangement, which becomes a fundamental stabilizing and orienting interaction of the crystal growth along with **c**. This different intermolecular interaction capacity between the isomers should be further analyzed by studying each isomer's Hirshfeld surface and molecular electrostatic potentials.

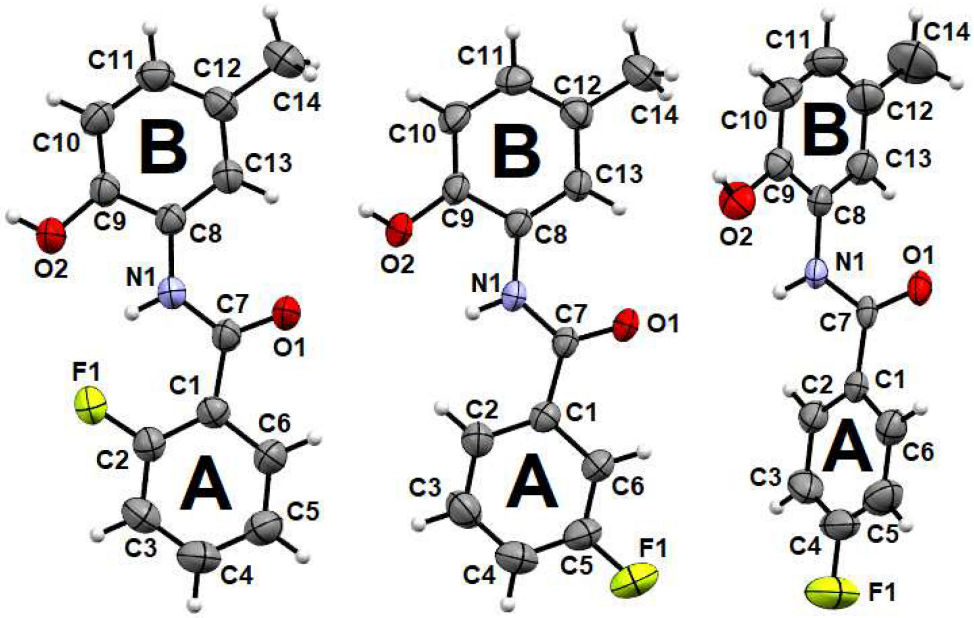

Figure 1. Ortep diagram of the ***o*-FPhB**, ***m*-FPhB**, and ***p*-FPhB**. Non-hydrogen atoms are drawn as 50% probability ellipsoids and hydrogen atoms as small spheres of arbitrary size.

Table 1. Hydrogen-bond geometry (Å, º).

Isomer	D-H···A	D-H	H···A	D···A	D-H···A
	O2-H02···O1 [i]	0.87(3)	1.78(3)	2.6402(16)	170(3)
	C6-H6···O2 [ii]	0.93	2.52	3.394(2)	156.2
***o*-FPhB**	C5-H5···F1 [ii]	0.93	2.96	3.632(2)	130.7
	C2-F1···Cg1			3.6441(13)	
	N1-H1···F1	0.86	1.99	2.6974(15)	138.6
	O2-H02···O1 [iii]	0.80(3)	1.85(3)	2.6454(18)	175(3)
***m*-FPhB**	C6-H6···O2 [iv]	0.93	2.52	3.376(2)	152.9
	C14-H141···F1 [v]	0.96	2.67	3.385(3)	131.4
	C7-O1···Cg1			3.8939(17)	
	C5-F1···Cg2			3.583(2)	
	N1-H1···O1 [vi]	0.86	2.01	2.807(3)	153.9
***p*-FPhB**	C5-H5···F1 [vii]	0.93	2.58	3.499(5)	169.6
	O2-HO2···O1 [viii]	0.87(5)	1.87(3)	2.663(3)	152(4)
	C2-H2···O2 [ix]	0.93	2.58	3.499(4)	169.9

[i]: x − 1, y, z; [ii]: x + 1, y, z; [iii]: x + 1, y, z; [iv]: x − 1, y, z; [v]: −x + 3/2, y + $\frac{1}{2}$, −z + 3/2; [vi]: x, −y + $\frac{1}{2}$, +z − $\frac{1}{2}$; [vii]: −x, +y + $\frac{1}{2}$, −z + $\frac{1}{2}$; [viii]: x, −y + 3/2, +z − $\frac{1}{2}$; [ix]: x, +y − 1, +z.

Crystal Data

For all: $C_{14}H_{12}FNO_2$, M = 245.25 g/mol, monoclinic, Z = 4, T = 295 K, refined parameters = 167.

For ***o*-FPhB**, space group $P2_1/n$, a = 7.3162(2) Å, b = 21.8636(6) Å, c = 7.8100(2) Å, β = 110.721(2)º, V = 1168.47(6) $Å^3$, μ(MoK_α) = 0.104 mm^{-1}, Dcalc = 1.394 Mg/m^3, 8233 reflections measured, 2389 unique, Rint = 0.0216. The final R1 was 0.0449 (I > 2_(I)) and wR2 was 0.1196 (all data), S = 1.036. Correctness of the model was confirmed by low residual peaks (0.191) and holes (−0.244) e.$Å^{-3}$.

For ***m*-FPhB**, space group $P2_1/n$, a = 7.3676(2) Å, b = 22.2728(7) Å, c = 7.6478(3) Å, β = 110.510(1)º, V = 1175.43(7) $Å^3$, μ(MoK_α) = 0.104 mm^{-1}, Dcalc = 1.386 Mg/m^3, 8383 reflections measured, 2394 unique, Rint = 0.0175. The final R1 was 0.0511 (I > 2_(I)) and wR2 was 0.1501 (all data), S = 1.055. Residual peaks (0.503) and holes (−0.327) e.$Å^{-3}$.

For ***p*-FPhB**, space group $P2_1/c$, a = 24.512(3) Å, b = 5.4218(8) Å, c = 9.3715(12) Å, β = 93.896(7)º, V = 1242.6(3) $Å^3$, μ(MoK_α) = 0.098 mm^{-1}, Dcalc = 1.311 Mg/m^3, 6008

reflections measured, 2016 unique, Rint = 0.0381. The final R1 was 0.0620 (I > 2_(I)) and wR2 was 0.1599 (all data), S = 1.124. Residual peaks (0.170) and holes (−0.252) e.Å^{-3}.

2.2. Supramolecular Features

2.2.1. ***o*-FPhB**

The supramolecular propagation of ***o*-FPhB** is shown in Figure 2. Relatively strong hydrogen bond interactions [11] are observed in this structure. In detail, the O2-HO2 group in the molecule at (x, y, z) acts as a hydrogen bond donor to O1 in the molecule at (x − 1, y, z). This interaction is supported by C6-H6···O2 hydrogen bonds, where the C6-H6 group in the molecule at (x, y, z) also acts as a hydrogen bond donor to the O2 atom in the molecule at (x + 1, y, z). Combined, these interactions form $R^2_2(7)$ rings [12] that link through the mutually anti carbonyl and hydroxy groups of the central molecule to form a 1-dimensional hydrogen-bonded chain that propagates along [100]. The conformational relationship between the fluorine atom and the carbonyl group is also anti. This structural characteristic enables the formation of the intramolecular N1-H1···F1 bond and the formation of the S(6) ring. The $R^2_2(7)$ and S(6) synthons guarantee the planarity observed between planes **A** and **B**, as shown in Figure 2. In this type of amide compound, N-H···O bonds would be expected. However, they do not occur due to steric hindrance, which is revealed by the proximity of the fluorine and hydroxyl group that does not allow the N-H group to form these bonds. Partial overlap of the benzene rings, which are at a distance between their centroids of 4.315 Å, and the fluorine atoms actively participate by forming halogen interactions, C-F···π, is observed (Table 1). The mean plane of the central amide moiety, C1-C7(O1)-N1-C8 (r.m.s. deviation = 0.019 Å), subtends dihedral angles of 4.76(9)° and 6.12(8)° with the **A** and **B** rings, respectively. It is known that the electronegativity of fluorine, its low polarizability, and its high capacity to attract free electronic pairs [13], empowers it to find interactions with other atoms and that, where these are strong enough, these interactions can strongly influence the process of crystalline growth, or the conformational structure adopted. The latter case seems to be true of ***o*-FPhB** and of crystals of other N-(2-fluorophenyl) amide molecules, where intramolecular N-H···F bonds form five-membered rings [14,15] that force planarity on the molecules.

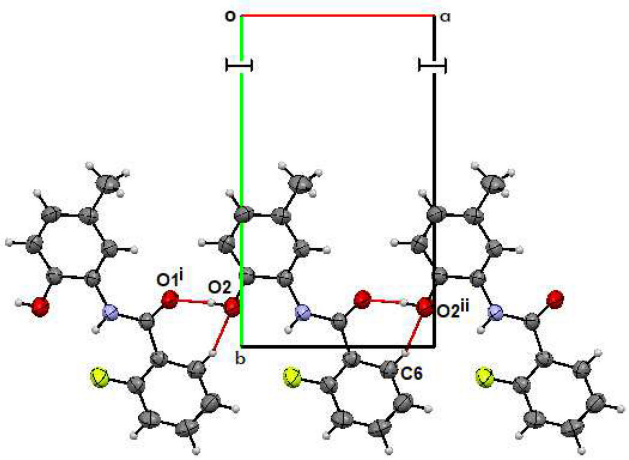

Figure 2. Crystal packing of ***o*-FPhB** seen along [001].

2.2.2. ***m*-FPhB**

Part of the supramolecular structure of ***m*-FPhB** is shown in Figure 3. As with the structure of ***o*-FPhB**, relatively strong O2-HO2···O1^{iii} hydrogen bonds, supported by intermolecular C6-H6···O2^{iv} hydrogen bond contacts, form $R^2_2(7)$ rings that link through the *anti* carbonyl and hydroxy groups to form a one-dimensional chain parallel to [100], see Table 1 for details. Unlike ***o*-FPhB**, the N-H donor can no longer create an intramolecular interaction with F1. Instead, an additional weak intermolecular hydrogen bond, C14-

H142···F1^{v}, links the one-dimensional chains parallel to the [010] direction, forming $R^4_4(29)$ edge-fused rings. The C14-H14 group in the molecule at (x, y, z) acts as a hydrogen bond donor to F1 in the molecule at $(-x + 3/2, y + \frac{1}{2}, -z + 3/2)$. With no intramolecular hydrogen bond as seen for ***o*-FPhB**, the structure of ***m*-FPhB** is free to adopt a different conformation with F and carbonyl groups, mutually *syn*. Despite the absence of the intramolecular interaction, the presence of the $R^2_2(7)$ synthons structure ***m*-FPhB** and in ***o*-FPhB** seems to be sufficient for the molecules to retain a planar conformation to prevent the formation of N-H···O bonds, which are characteristic of amide compounds.

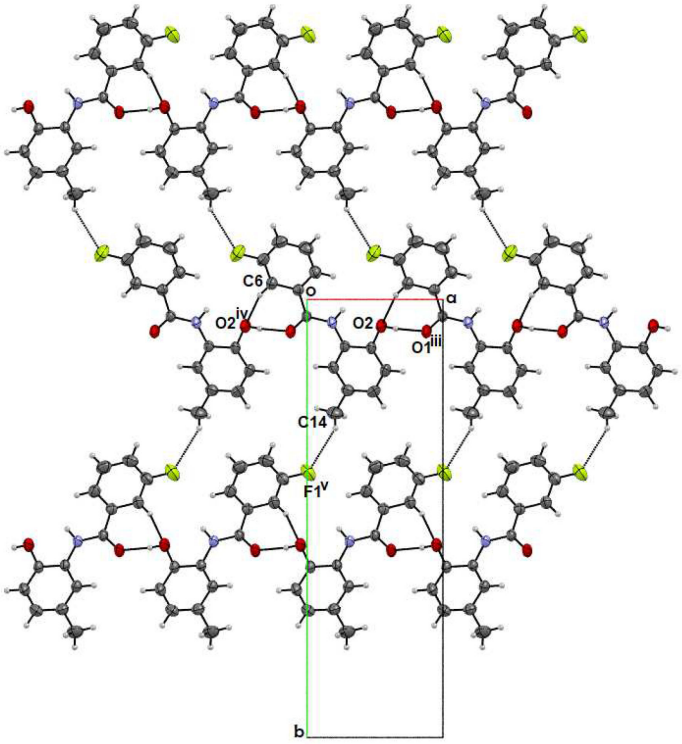

Figure 3. Crystal packing of ***m*-FPhB** seen along [001].

The mean plane of the central amide moiety (r.m.s. deviation = 0.024 Å) shows dihedral angles of 1.651(1)º and 5.491(9)º with the **A** and **B** rings, respectively. Both ***o*-FPhB** and ***m*-FPhB** share many structural features with non-fluorinated, **FPhB** [7]. Comparison of the unit cell parameters, identical space groups, similar bond lengths, and bond angles, the planarity of the molecules, and the retention of the core $R^2_2(7)$ based hydrogen-bonding motif of ***o*-FPhB** shows a great closeness between these systems. The structural behavior of ***m*-FPhB** can also be compared with that of the related compound 3-chloro-*N*-(3-chlorophenyl)benzamide (CPB) [16]. The structure of CPB has similar bond parameters to ***m*-FPhB**, but its structure is otherwise different, with two independent molecules per asymmetric unit and a torsion angle of approximately 35° for the central amide C-N-(C=O)-C segment.

An essential feature in ***m*-FPhB** is based on the overlapping of the benzene rings, where the fluorine and carbonyl groups actively participate, forming C-F···Cg2 and C-O···Cg1 interactions (Figure 4), managing to consolidate further the molecular arrangement leading to the formation of sheets running parallel to the planes of the benzene rings shown in Figure 3.

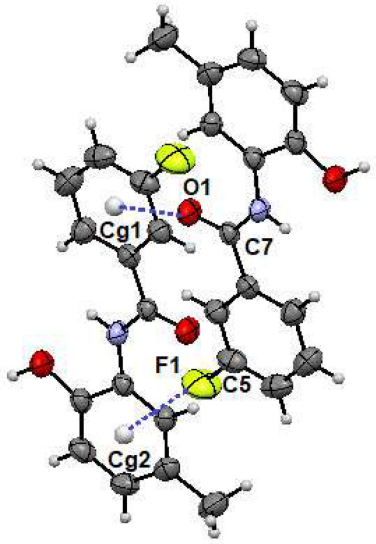

Figure 4. C-O···Cg and C-F···Cg interactions in ***m*-FPhB** are highlighted in dashed blue lines.

2.2.3. ***p*-FPhB**

The structural conformation of ***p*-FPhB** presents marked differences from isomers ***o*-FPhB**, and ***m*-FPhB**, notably by forming a dihedral angle between the rings of nearly 90°. The mean plane of the central amide moiety (r.m.s. deviation = 0.0064 Å) shows dihedral angles of 26.28(16)° and 70.28(9)° with the **A** and **B** benzene rings, respectively.

As shown in Figure 5, in contrast to ***o*-FPhB** and ***m*-FPhB**, in ***p*-FPhB**, the C6-H6···O2 bond is not observed, thus indicating the disappearance of the $R^2_2(7)$ rings, distorting the properties of the peptide bond and losing its planarity, its double bond character, its resonance and at the same time becoming more susceptible to nucleophilic or electrophilic attacks that are reflected in the appearance of the N-H···O bonds typical of structures with activated peptide bonds. This new organization in ***p*-FPhB** takes advantage of the N-H donor to form a relatively strong N1-H1···O1^{vi} interaction, where the N1-H1 group in the molecule at (x, y, z) acts as a hydrogen bond donor to the O1^{vi} atom in the molecule at (x, $-$y+ $\frac{1}{2}$, +z $-$ $\frac{1}{2}$). The amide oxygen atom also accepts a second relatively strong hydrogen bond, O2-H02···O1^{viii}, supported by the short contact C2-H2···O2^{ix}. Here the hydroxyl O2-H02 group in the molecule at (x, y, z) acts as a hydrogen bond donor to O1 in the molecule at (x, $-$y+3/2, +z $-$ $\frac{1}{2}$), and the C2-H2 group in the molecule at (x, y, z) acts as a donor to hydroxyl O2 in the molecule at (x, +y$-$1, +z), see Table 1 for details. These interactions combine to form chains of molecules running along [001]. The F atom accepts a weak hydrogen-bonded contact, a C5-H5···F1^{vii} interaction, where the C5-H5 group at (x, y, z) acts as a hydrogen bond donor for the F1^{vii} atom in the molecule at ($-$x, + y + $\frac{1}{2}$, $-$z + $\frac{1}{2}$). These last interactions form edge-fused R^4_4 (28) rings running along [001]. In contrast to the ***o*-FPhB** and ***m*-FPhB** compounds, halogen bonds are not observed in ***p*-FPhB**. The approximately planar behavior of compounds ***o*-FPhB** and ***m*-FPhB** enables their growth in the form of layers. However, in ***p*-FPhB**, the molecule is folded, and this factor causes the entire crystal lattice to wrap. The C7-N1-C8-C13 torsion angle is the most sensitive to the position changes of the fluorine substituent in the benzamide ring, indicating that the value of the torsion angle changes abruptly for a ***p*-FPhB** molecule. Similar amide systems, such as 2-chloro-4-fluoro-N-phenyl benzamide [17] and 4-Bromo-N-phenyl benzamide [18], show similar behavior.

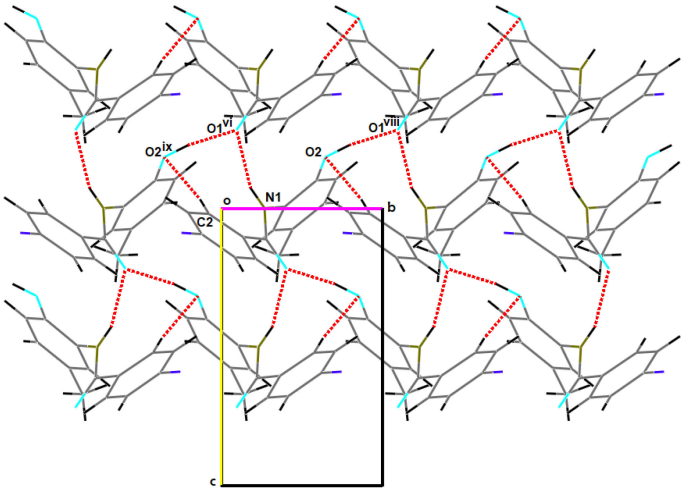

Figure 5. Part of the crystal structure of ***p*-FPhB** shows the formation of $R^2_3(9)$ and $R^3_3(17)$ edge-fused rings and a chain of molecules running along [001].

2.3. Analysis of the Hirshfeld Surfaces

The Hirshfeld surface analysis of the three compounds is presented in detail in the supplementary section. Different behavior of fingerprints of the isomers involving C···C can be visualized in Figure 6 by the cyan-colored area, demonstrating the disappearance of molecular growth in layers for ***p*-FPhB**.

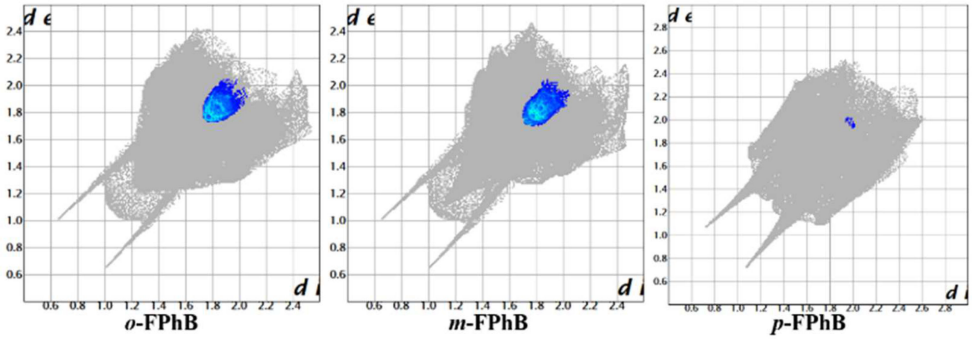

Figure 6. Fingerprints of the C···C interaction for ***o*-FPhB**, ***m*-FPhB**, and ***p*-FPhB**.

2.4. UV-Vis

The UV spectra of the three compounds show absorption bands at λ = 304, λ = 299, and λ = 298 nm, respectively, in acetonitrile. The most intense bands obtained near this region in B3LYP/6–311G(d,p) calculations for the ***o*-FPhB**, ***m*-FPhB**, and ***p*-FPhB** isolated isomers show absorption bands at λ = 329.32 nm, λ = 305.39 nm, and λ = 317.44 nm, respectively. These bands are attributed to an intramolecular charge transfer (ICT) from the highest occupied molecular orbital (HOMO) to the lowest unoccupied molecular orbital (LUMO). The HOMO-LUMO energy difference (ΔE), a measure of intramolecular charge transfer, can become significant when analyzing biological activities in many unsaturated systems [19]. Theoretical calculations performed on isomers ***o*-FPhB**, and ***m*-FPhB** showed a HOMO-LUMO energy gap of 4.2463 and 4.0598 eV, respectively. At the same time, ***p*-FPhB** reveals a higher energy gap value (4.4746 eV) resulting from the loss of planarity of the peptide bond, which also leads to a loss in its conjugation property. These results are in agreement with the experimental values.

These values were obtained using the time-dependent density functional theory (TD-DFT). They represent the energy needed for electronic excitation, which belongs mainly to the π-π* transition. According to Figure 7, the HOMO shows charge density localized over

the hydroxy-methylbenzamide ring and the central amide segment. The molecular orbital LUMO has a charge distributed over the entire molecule, except over the hydroxyl group. This behavior suggests a transfer of a pair of electrons starting from the oxygen atom of the hydroxyl group and oriented by conjugation to the fluoro-phenyl ring, forming resonant structures between these states.

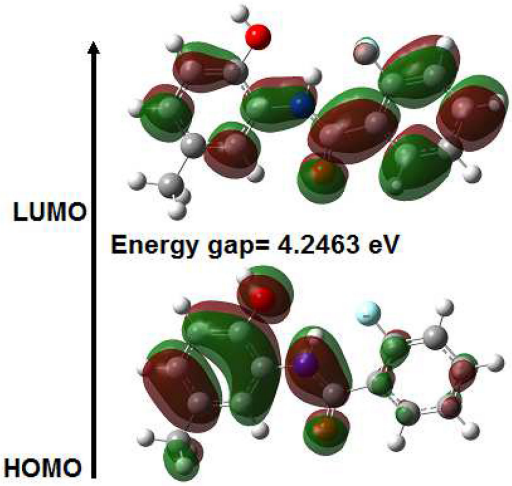

Figure 7. Electron distribution of the HOMO and the LUMO energy levels for ***o*-FPhB**.

2.5. Molecular Electrostatic Potential (MEP)

MEP is an effective tool in quantum chemistry to understand and visualize the structure–activity relationships of molecules [20]. The calculation of electrostatic potentials defines the electron density in different regions of the molecule, whose quantitative potential values are fundamental to know the sites where an electrophilic attack can occur or nucleophilic reactions can take place, as well as the hydrogen-bonding interactions [21]. This tool enables molecular recognition in one molecule's active environments by analyzing possible enzyme–substrate or drug–receptor interactions through each molecule's potential. The study of MEP for the three compounds was conducted using the Gauss09W [22] to obtain a qualitative analysis, and the Multiwfn 3.6 program was used for quantitative analysis of the surface [23]. On the potential surface (Figure 8), two zones marked in dark blue and corresponding to positive regions of low electron density show potentials of 49.19 and 27.49 kcal mol^{-1} for ***o*-FPhB** and 50.22 and 40.90 kcal mol^{-1} for ***p*-FPhB**. The highest maximum potential values in ***o*-FPhB** and ***m*-FPhB** show regions that accommodate the strongest hydrogen interactions O2-HO2···O1, along with C2-H2···O2, which involves the formation of R^2_2 (7) rings in each isomeric structure (see Table 1), where the formation of this synthon in crystal growth is critical in defining the quasi planar conformation of the molecules. The lower potential values for each compound should accommodate regions that would facilitate N-H···O interactions. The structural conformations of ***o*-FPhB** and ***p*-FPhB** coincided well with those obtained experimentally. However, for ***m*-FPhB**, the calculations showed essential differences in their molecular conformation, revealing a result a little distance from the planarity between the rings. Thus, the experimental data show, from Table 1 and supramolecular analysis, the formation of R^2_2 (7) rings that guarantee molecular planarity in ***o*-FPhB** and ***m*-FPhB**. In contrast to these results, in ***p*-FPhB**, relatively high potential in the NH group region stereochemically reinforces the activation of strong N1-H1···O1 hydrogen bonds, motivated by their molecular non-planarity.

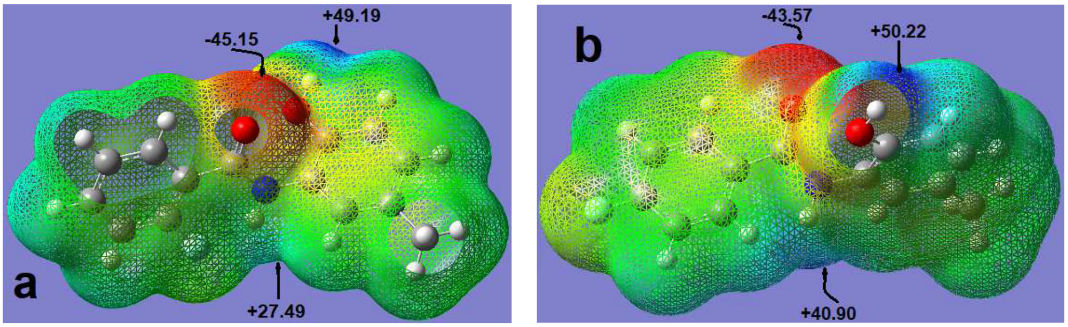

(**a**) (**b**)

Figure 8. Three-dimensional representation of the electrostatic potential around the molecules (**a**) ***o*-FPhB**; (**b**) ***p*-FPhB**. Values are given in kcal/mol.

2.6. Docking Studies

To compare the potential biological properties of the isomers, a molecular simulation was carried out in which the conformational structures of the three isomers were subjected to a molecular docking study. For this purpose, the "SwissTargetPrediction" program was used as a molecular target finder, and two receptors of the VEGFR (vascular endothelial growth factor) protein were chosen as "molecular targets.". These receptors are essential in different processes, such as angiogenesis, vasculogenesis, and lymphangiogenesis [24]. In the molecular docking calculations, the Auto Dock Vina program was used [25]. In preparing of receptors and ligands, the 3D structure of VEGFR-1 and VEGFR-2 was selected from the Protein Databank under ID 3HNG [26] and 3U6J [27], respectively. Auto Dock Tools program [28] prepared the target molecular structure by removing water molecules and adding hydrogen atoms. The programs Chimera [29] and LigPlot+ [30], multiple ligand–protein interaction diagrams for drug discovery, were used to visualize the results. From the docking simulations, the results obtained with a drug known as axitinib with antiangiogenic activity [24] were compared with the results obtained with the three benzamide isomers (see Supplementary Part S3). In these calculations, the interactions of some protein residues with the molecules under study were found to occur in the active center of the target protein. The benzamide isomers showed the formation of hydrogen bonds with the target proteins, one of which was also observed in the calculations with the reference compound axitinib. All three isomers revealed similar behavior, energetic affinities, and binding distance calculations between the protein targets VEGFR-1 and VEGFR-2. The interactions of ***m*-FPhB** can be visualized in Figure 9. A hydrogen bond is observed between the hydroxyl group of glutamic acid and the O2 of the hydroxyl group of the ***m*-FPhB** isomer.

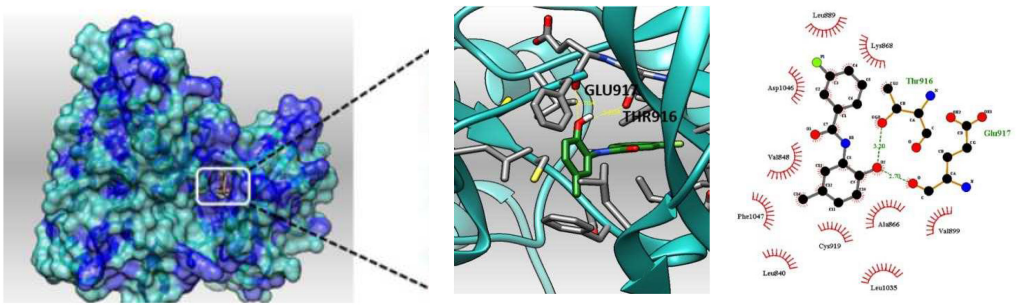

(**a**) (**b**) (**c**)

Figure 9. Interactions of the different isomers with the VEGFR-2 receptor. (**a**) The hydrophobic residues of the protein target are shown in dark blue tones. (**b**) The ***m*-FPhB** compound interacts with the GLU917 protein residue. (**c**) The representation in LigPlot^{+} presents the hydrophobic residues with red lines and hydrogen interactions with a dotted green line.

This interaction also occurs when the axitinib acts as an inhibitor. Visualization of possible bonds involving fluorine atoms was not possible at this level of methodology. The calculations made by molecular simulation show more or less similar results for the three compounds under study with lower protein–ligand interaction energy values than that presented by the drug axitinib (see Supplementary Part S3).

3. Materials and Methods

3.1. General Information

The melting point was determined on a Büchi melting point B-450 apparatus (Instrumart, South Burlington, VT, USA). IR spectra were recorded on a Shimadzu FTIR 8400 spectrophotometer (Scientific Instruments Inc., Seattle, WA, USA) using KBr disks. UV-Vis spectra were recorded with a Shimadzu UV-1700 PharmaSpec spectrophotometer at 190 to 900 nm (Scientific Instruments Inc., Seattle, WA, USA) (see Supplementary Part S2). The starting 2-amino-4-methyl phenol, 2-fluorobenzoyl chloride, and acetonitrile were purchased from Sigma-Aldrich (San Luis, MO, USA); they were analytical grade reagents, and further purifications were unnecessary. The 2-amino-4-methyl phenol (0.100 g, 0.812 mmol) was dissolved in acetonitrile (15 mL) prior to the subsequent slow addition of 2-fluorobenzoyl chloride (0.130 g, 0.820 mmol). The solution was refluxed at 85 °C for 3 h, producing a pink solid. Silica gel aluminum plates (Merck 60 F254, Darmstadt, Germany) were used for analytical TLC. At the end of the reaction, the solid was filtered hot. Finally, at room temperature, the filtrate was recrystallized from methanol via slow evaporation of the solvent over three days, achieving a yield of 60%. Excellent crystals of ***o*-FPhB** were obtained, M.P. 181(1) °C. This same synthetic method was used with the appropriate fluorobenzoyl isomers to obtain the ***m*-FPhB** (0.125 g, 0.510 mmol, 63% yield), M.P. 187(1) °C and the ***p*-FPhB** benzamide compounds (0.110 g, 0.449 mmol, 55% yield). M. P. 179(1) °C. FTIR-ATR for ***o*-FPhB**: ν = 3387 (N-H), 3107 (O-H), 1647 (C=O), 1612 (C=C), 1199 (C-F); for ***m*-FPhB** ν = 3388 (N-H), 3153 (O-H), 1638 (C=O), 1615 (C=C), 1207 (C-F); for ***p*-FPhB** ν = 3397 (N-H), 3196 (O-H), 1636 (C=O), 1619 (C=C), 1223 (C-F).

3.2. Computational Methods

Theoretical calculations were performed at DFT/B3LYP level with 6-311G(d,p) basis sets to predict the molecular structure and vibrational wavenumbers using the Gaussian 09 program [21]. The B3LYP represents Becke's three-parameter hybrid functional method [31] with Lee–Yang–Parr's correlation functional (LYP) [32]. For the assignments of the calculated wavenumbers, the Gaussview 5.0 program was used to obtain a visual representation of the vibration modes [33]. The potential energy distribution (PED) was calculated with the VEDA 4 program package [34]. Stationary points on the potential energy surface were fully optimized, and harmonic vibration frequencies were evaluated to characterize their nature as minima. The absence of imaginary frequencies indicated that all optimized structures were the true minimum. Atomic coordinates from crystallographic structural data were used as initial parameters in the computation of the minimum-energy conformation of the compounds.

3.3. Refinement

All H atoms were found in a Fourier difference map, but they were placed in geometrically idealized positions, with C-H = 0.93 Å (ring), 0.96 Å (methyl), and N-H = 0.86 Å, and they were refined using a riding-model approximation, with $U_{iso}(H) = 1.2U_{eq}(C, N)$ for the aromatic and amine or $1.5U_{eq}(C)$ for the methyl groups, respectively.

4. Conclusions

The synthesis of isomers ***o*-FPhB**, ***m*-FPhB**, and ***p*-FPhB** by a nucleophilic substitution reaction was successfully performed, and it enabled the identification of critical structural affinities and differences. Their supramolecular study verifies the presence of $R^2_2(7)$ synthons in ***o*-FPhB** and ***m*-FPhB**, inducing planarity in the molecule. In ***o*-FPhB**, this planarity

is reinforced by forming intramolecular rings (S6), in which the fluorine atom participates. Compound ***p*-FPhB** moves away from this tendency, opening a stereochemical gate to activate the N-H···O interpeptide bond, thus defining its supramolecular and biological properties. The supramolecular study of the three compounds showed the active participation of fluorine atoms in assembling their structures, either by forming intramolecular rings or by creating chains of molecules during crystal growth. Analysis of the molecular parameters showed that the C7-N1-C8-C13 torsion angle is the most sensitive to positional changes of the fluorine atom on the benzamide ring. To order their molecules in the form of parallel sheets, **o-FPhB** and ***m*-FPhB** compounds develop hydrogen C-H···Cg, halogen C-F···Cg, or C=O···Cg interactions. This behavior is not revealed in ***p*-FPhB**. The theoretical evaluation of the properties of the compounds shows good agreement with the experimental values. The observed vibrational frequencies reaffirm the presence of functional groups of interest, such as N-H, C=O, O-H, C-F, C-H, and aromatic rings. In the UV-Vis region, higher energetic stability, an increase in the Hirshfeld surface due to O···H interactions, and an increase in the electrostatic potential in the NH region, concerning its isomers, reaffirms the disposition of ***p*-FPhB** for the formation of the N-H···O interpeptide bond. Finally, a molecular docking study of the benzamides under investigation, with protein receptors related to the vascular endothelial growth factor VEGFR-1 and VEGFR-2, showed similar behavior for all three isomers without highlighting any substantial difference between these interactions by the position of the fluorine atom in the ring.

Supplementary Materials: Supplementary data for ***o*-FPhB**, ***m*-FPhB**, and ***p*-FPhB** have been deposited at the Cambridge Crystallographic Data Centre. (CCDC 1829136, 1829137, and 1829138 contain the supplementary crystallographic data for this paper. These data can be obtained free of charge via http://www.ccdc.cam.ac.uk (or E-mail: deposit@ccdc.cam.ac.uk)).

Author Contributions: N.M.-O. performed the chemical synthesis and carried out compound characterization. J.C.T., J.E., A.R.K. carried out the X-ray analysis and solved the structure. R.M.-F. performed the theoretical work, wrote the manuscript. All authors have read and agreed to the published version of the manuscript.

Funding: This research received no external funding.

Institutional Review Board Statement: Not applicable.

Informed Consent Statement: Not applicable.

Data Availability Statement: Not applicable.

Acknowledgments: RMF is grateful to the Universidad del Valle, Colombia, for partial financial support and its support in realizing his sabbatical year. (CI project 71169).

Conflicts of Interest: The authors declare no conflict of interest.

Sample Availability: Samples of the compounds are currently unavailable due to the degradation of the precursors during the COVID-19 pandemic.

References

1. Ji, X.-Y.; Wang, H.-Q.; Hao, L.-H.; He, W.-Y.; Gao, R.-M.; Li, Y.-P.; Li, Y.-H.; Jiang, J.-D.; Li, Z.-R. Synthesis and antiviral activity of *N*-phenylbenzamide derivatives, a novel class of enterovirus 71 inhibitors. *Molecules* **2013**, *18*, 3630–3640. [CrossRef] [PubMed]
2. Ogawa, Y.; Tokunaga, E.; Kobayashi, O.; Hirai, K.; Shibata, N. Current contributions of organofluorine compounds to the agrochemical industry. *iScience* **2020**, *23*, 101467. [CrossRef] [PubMed]
3. Berkowitz, D.B.; Karukurichi, K.R.; de la Salud-Bea, R.; Nelson, D.L.; McCune, C.D. Use of fluorinated functionality in enzyme inhibitor development: Mechanistic and analytical advantages. *J. Fluor. Chem.* **2008**, *129*, 731–742. [CrossRef] [PubMed]
4. Filler, R.; Saha, R. Fluorine in medicinal chemistry: A century of progress and a 60-year retrospective of selected highlights. *Future Med. Chem.* **2009**, *1*, 777–791. [CrossRef] [PubMed]
5. Biffinger, J.C.; Kim, H.W.; DiMagno, S.G. The polar hydrophobicity of fluorinated compounds. *ChemBioChem* **2004**, *5*, 622–627. [CrossRef] [PubMed]
6. Berkowitz, D.B.; Bose, M. (α-Monofluoroalkyl)phosphonates: A class of iso-acidic and "tunable" mimics of biological phosphates. *J. Fluor. Chem.* **2001**, *112*, 13–33. [CrossRef]

7. Moreno-Fuquen, R.; Mariño, N.J.; Kennedy, A.R. Crystal structure of N-(2-hydroxy-5-methylphenyl)benzamide. *Acta Crystallogr. E: Crystallogr. Commun.* **2015**, *71*, o943. [CrossRef]
8. Montalbetti, C.A.G.N.; Falque, V. Amide bond formation, and peptide coupling. *Tetrahedron* **2005**, *61*, 10827–10852. [CrossRef]
9. Spackman, M.A.; Jayatilaka, D. Hirshfeld surface analysis. *CrystEngComm* **2009**, *11*, 19–32. [CrossRef]
10. Farrugia, L.J. WinGX and ORTEP for windows: An update. *J. Appl. Cryst.* **2012**, *45*, 849–854. [CrossRef]
11. Emsley, J. The composition, structure and hydrogen bonding of the β-diketones. In *Structure and Bonding*; Cardine, C., Ed.; Springer: Berlin/Heidelberg, Germany, 1984; Volume 57, pp. 147–191.
12. Bernstein, J.; Davis, R.E.; Shimoni, L.; Chang, N.-L. Patterns in hydrogen bonding: Functionality and graph set analysis in crystals. *Angew. Chem. Int. Ed. Engl.* **1995**, *34*, 1555–1573. [CrossRef]
13. Dunitz, J.D. Organic fluorine: Odd man out. *ChemBioChem* **2004**, *5*, 614–621. [CrossRef] [PubMed]
14. Büyükgüngör, O.; Odabaşoğlu, M. 2-Fluoroanilinium N-(2-fluorophenyl)oxamate. *Acta Crystallogr. E: Crystallogr. Commun.* **2008**, *64*, o808. [CrossRef] [PubMed]
15. Barbarich, T.J.; Rithner, C.D.; Miller, S.M.; Anderson, O.P.; Strauss, S.H. Significant inter- and intramolecular O−H···FC hydrogen bonding. *J. Am. Chem. Soc.* **1999**, *121*, 4280–4281. [CrossRef]
16. Gowda, B.T.; Foro, S.; Sowmya, B.P.; Fuess, H. 3-Chloro-N-(3-chlorophenyl)benzamide. *Acta Crystallogr. E: Crystallogr. Commun.* **2008**, *64*, o949. [CrossRef]
17. Tan, Z.; Bing, Y.; Fang, S.; Kai, Z.; Yan, Y. 2-Chloro-4-fluoro-N-phenylbenzamide. *Acta Crystallogr. E: Crystallogr. Commun.* **2009**, *65*, o1757. [CrossRef]
18. Fun, H.-K.; Chantrapromma, S.; Sripet, W.; Ruanwas, P.; Boonnak, N. 4-Bromo-N-phenylbenzamide. *Acta Crystallogr. E: Crystallogr. Commun.* **2012**, *68*, o1269–o1270. [CrossRef]
19. Fukui, K.; Yonezawa, T.; Shingu, H.J. A Molecular orbital theory of reactivity in aromatic hydrocarbons. *J. Chem. Phys.* **1952**, *20*, 722–725. [CrossRef]
20. Politzer, P.; Truhlar, D.G. *Chemical Applications of Atomic and Molecular Electrostatic Potentials*; Plenum Press: New York, NY, USA, 1981; pp. 1–6.
21. Politzer, P.; Murray, J.S. The fundamental nature and role of the electrostatic potential in atoms and molecules. *Theor. Chem. Acc.* **2002**, *108*, 134–149. [CrossRef]
22. Frisch, M.J.; Trucks, G.W.; Schlegel, H.B.; Scuseria, G.E.; Robb, M.A.; Cheeseman, J.R.; Scalmani, G.; Barone, V.; Petersson, G.A.; Nakatsuji, H.; et al. *Gaussian 09, Revision B. 01.*; Gaussian Inc.: Wallingford, CT, USA, 2009.
23. Lu, T.; Chen, F. Multiwfn: A multifunctional wavefunction analyzer. *J. Comput. Chem.* **2012**, *33*, 580–592. [CrossRef] [PubMed]
24. Kelly, R.J.; Rixe, O. Axitinib—A selective inhibitor of the vascular endothelial growth factor (VEGF) receptor. *Target. Oncol.* **2009**, *4*, 297–305. [CrossRef] [PubMed]
25. Trott, O.; Olson, A.J. AutoDock Vina: Improving the speed and accuracy of docking with a new scoring function, efficient optimization, and multithreading. *J. Comput. Chem.* **2010**, *31*, 455–461. [CrossRef] [PubMed]
26. Tresaugues, L.; Roos, A.; Arrowsmith, C.H.; Berglund, H.; Bountra, C.; Collins, R.; Edwards, A.M.; Flodin, S.; Flores, A.; Graslund, S.; et al. Crystal structure of VEGFR1 in complex with N-(4-Chlorophenyl)-2-((pyridin-4-ylmethyl)amino)benzamide. *RCSB PDB* **2009**. [CrossRef]
27. Norman, M.H.; Liu, L.; Lee, M.; Xi, N.; Fellows, I.; D'Angelo, N.D.; Dominguez, C.; Rex, K.; Bellon, S.F.; Kim, T.S.; et al. Structure-based design of novel class II c-Met inhibitors: Identification of pyrazolone-based derivatives. *J. Med. Chem.* **2012**, *55*, 1858–1867. [CrossRef] [PubMed]
28. Morris, G.M.; Huey, R.; Lindstrom, W.; Sanner, M.F.; Belew, R.K.; Goodsell, D.S.; Olson, A.J. AutoDock4 and AutoDockTools4: Automated docking with selective receptor flexibility. *J. Comput. Chem.* **2009**, *31*, 2785–2791. [CrossRef] [PubMed]
29. Pettersen, E.F.; Goddard, T.D.; Huang, C.C.; Couch, G.S.; Greenblatt, D.M.; Meng, E.C.; Ferrin, T.E. UCSF Chimera—A visualization system for exploratory research and analysis. *J. Comput. Chem.* **2004**, *25*, 1605–1612. [CrossRef] [PubMed]
30. Laskowski, R.A.; Swindells, M.B. LigPlot+: Multiple ligand-protein interaction diagrams for drug discovery. *J. Chem. Inf. Model.* **2011**, *51*, 2778–2786. [CrossRef]
31. Becke, A.D. Density-functional exchange-energy approximation with correct asymptotic behavior. *Phys. Rev.* **1988**, *A38*, 3098–3100. [CrossRef] [PubMed]
32. Lee, C.; Yang, W.; Parr, R.G. Development of the Colle-Salvetti correlation-energy formula into a functional of the electron density. *Phys. Rev.* **1988**, *B37*, 785–789. [CrossRef]
33. Nielsen, A.B.; Holder, A.J. *Gauss View 5.0, User's Reference*; Gaussian Inc.: Pittsburgh, PA, USA, 2009.
34. Jamroz, M.H. Vibrational energy distribution analysis (VEDA): Scopes and limitations. *Spectrochim. Acta Part A Mol. Biomol. Spectrosc.* **2013**, *114*, 220–230. [CrossRef]